Journal of Engineering Physics and Thermophysics, Vol. 83, No. 6, 2010

INFLUENCE OF THE METHODS OF ENERGY ACTION ON DEFLAGRATION-TO-DETONATION TRANSITION

V. V. Golub, D. I. Baklanov, V. V. Volodin, and S. V. Golovastov

UDC 534.222.2+536.46+661.215.1

The results of experimental gas-detonation investigations carried out in the past decade at the Department of Physical Gasdynamics of the Joint Institute of High Temperatures of the Russian Academy of Sciences (JIHT RAS) in connection with the problems of creation of a pulse detonation engine have been presented. Consideration has been given to the influence of the shape of injectors on the formation of detonation in a gas flow with separate feed of the fuel and the oxidant, the influence of acoustic action on the ignition region, reduction in the predetonation length in the flow of a mixture capable of detonation, and improvement in the efficiency of electric-discharge initiation of detonation by the self-magnetic and induced external magnetic field.

Keywords: *detonation, mixing, injectors, acoustics, flow, magnetic field, electric discharge.*

Introduction. In 1952, T. V. Bazhenova and R. I. Soloukhin began a series of works investigating combustion and detonation in gaseous mixtures at the G. M. Krzhizhanovskii Institute of Power Engineering.

"Detonation waves represent a complex of interrelated physicochemical processes; therefore, the problem of detonation, in addition to its technical significance, attracts the attention of many researchers from different fields of knowledge. Establishment of thermodynamic equilibrium behind the detonation front, vibrations of the gas and spinning detonation, transition of slow combustion to detonation, detonation limits, combustion and detonation in supersonic gas flows — all these issues turned out to be related in a close manner to the distinctive features of shock waves, to the rates and mechanisms of chemical reactions, turbulence, acoustic oscillations, and other processes in gases.

The study of detonation was by no means confined to creation of a classical Chapman–Jouguet scheme. Wide variations from this scheme due to the peculiarities of the compatibility of physicochemical and hydrodynamic processes in the gaseous medium have long been evident" [1].

Almost half a century has passed since R. I. Soloukhin identified the topical problems of detonation theory, but most of these problems have not yet been solved, even at the current stage of development of science.

The topicality of investigation of gas detonation has strongly grown in recent decades in connection with the effort to create a pulse detonation engine [2]. The issue of energy utilization of the detonation burning of a fuel was first raised in 1940 by Ya. B. Zeldovich. However, no systematic study of detonation with the aim of using it in engines was made until the practical ways of improving jet engines based on deflagration burning were exhausted. Late in the twentieth century, possible methods of creation of pulse detonation engines began to be intensely investigated in many countries. This called for solution of both fundamental and applied problems of optimization of a detonation combustion chamber. In this paper, we give a review of investigations on deflagration-to-detonation transition that have been performed at the Department of Physical Gasdynamics of the JIHT RAS. The investigations were carried out in connection with the problems of creation of a pulse detonation engine.

Experimental Bench. The experimental bench on which the formation of detonation in the flow of fuel components not mixed in advance was investigated and which represented a detonation tube fitted with a system for feeding fuel components, an initiation system, a pressure chamber, an evacuation system, and a diagnostic system is presented in Fig. 1. The detonation combustion chamber (DCCh) was manufactured from stainless steel and had a circular cross section with an inside diameter of 83 mm and a length of 2.51 m. The fuel components were fed separately under pressure from buffer vessels. To obtain the necessary stoichiometric relation of the components and

Joint Institute of High Temperatures of the Russian Academy of Sciences, 13 Izhorskaya Str., Building 2, Moscow, 125412, Russia; email: golub@ihed.ras.ru. Translated from Inzhenerno-Fizicheskii Zhurnal, Vol. 83, No. 6, pp. 1157–1173, November–December, 2010. Original article submitted May 3, 2010.

1062-0125/10/8306-1227

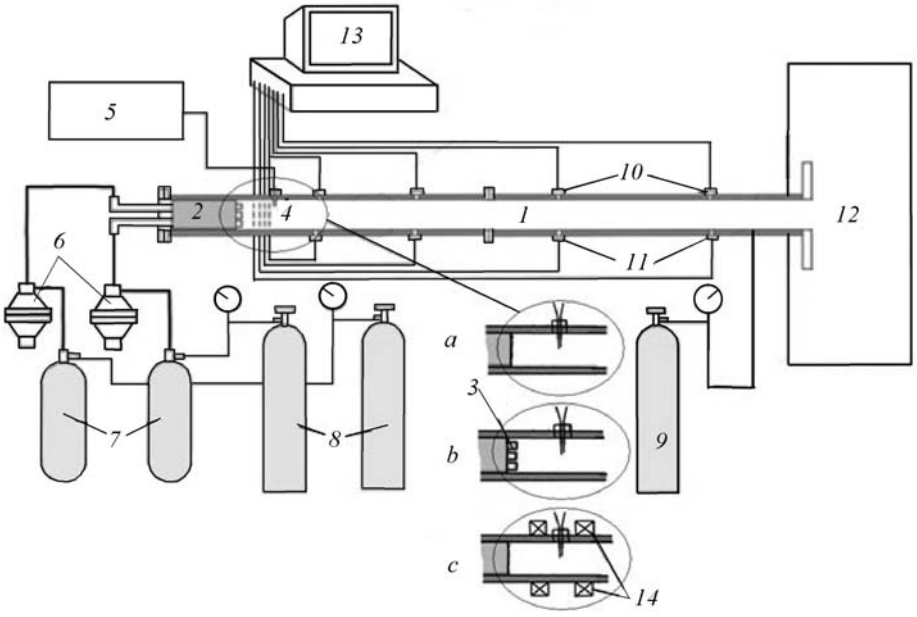

Fig. 1. Diagram of the experimental bench: 1) DCCh; 2) injector unit; 3) injectors; 4) spark discharger; 5) ignition unit; 6) pressure-operated electric valves; 7) buffer vessels; 8) cylinders with hydrogen and oxygen (air); 9) vessel with a premixed mixture; 10) RSV 113A piezoelectric pressure transducers; 11) FD-256 photodiodes; 12) damping vessel; 13) data-acquisition system; the diagrams of experiments on detonation formation in a quiescent mixture (a) and a moving mixture (b) and on studying the influence of a magnetic field on the initiation of detonation (c); 14) coils.

to ensure the corresponding flow rate of the fuel, the required pressure of the fuel and the oxidant was set in the buffer vessels before each experiment. An injector unit which could move past a spark discharge was installed in the closed DCCh end. In experiments with a quiescent mixture (a), the holes in the injector unit were plugged. In experiments with a moving mixture (b), the injectors were installed. Coils for studying the influence of a magnetic field on the initiation of detonation were arranged on the exterior DCCh surface (c). The opposite end of the DCCh was connected to a damping vessel. RSV 113A34 piezoelectric pressure transducers and FD-256 photodiodes were installed along the DCCh for recording shock and detonation waves in successive DCCh cross sections. In the experiments, the DCCh was preevacuated by NVR-5D pumps to a pressure of 10–30 mm Hg or remained filled with air at atmospheric pressure.

The detonation-initiation system represented a three-electrode spark discharger with a grounded electrode, an electrode connected to a capacitor of capacitance 0.1, 4, 100, and 200 μF (depending on the required initiation energy), and a control electrode on which the signal from the automobile ignition coil was fed. The energy stored in the capacitor varied from 0.5 to 1200 J. The fraction of the energy stored in the capacitor, which was released in the spark discharge, amounted to approximately 25%.

Influence of the Injector Shape on the Formation of Detonation in the Gas Flow with Separate Feed of the Fuel and the Oxidant. Improvement of mixing is an important element contributing to the formation of detonation with separate feed of the fuel and the oxidant in both a pulse regime and a continuous regime. Gas flow out of injectors determines in many respects the quality of mixing of the fuel components. Furthermore, the interaction of the ambient and injected gases determines mixing in the boundary layer. Development of the boundary layer of the gas jet can be controlled, since there are large-scale vortex structures in the boundary layer and they interact with perturbations in the flow [3].

The structure of flow of the fuel components out of the injectors was visualized in advance. Experiments on visualization of flow of noncombustible gases from injectors of different types were conducted on a UT-2M shock

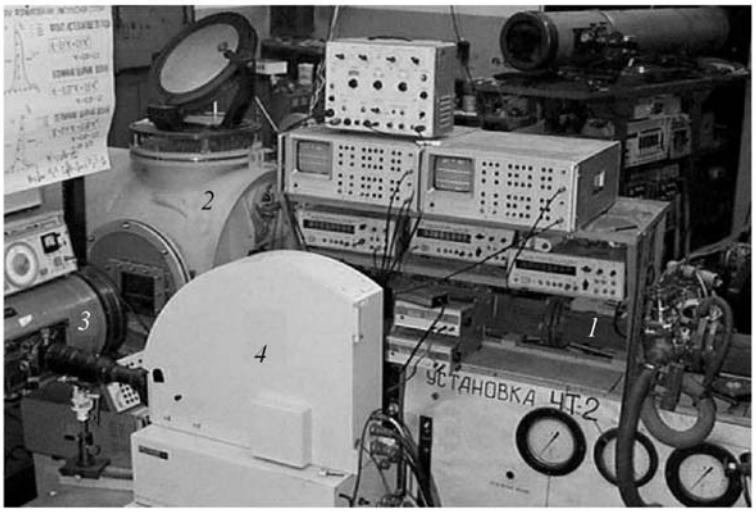

Fig. 2. UT-2M shock tube: 1) shock tube; 2) pressure chamber; 3) IAB-451 shadow device; 4) VSK-5 chamber.

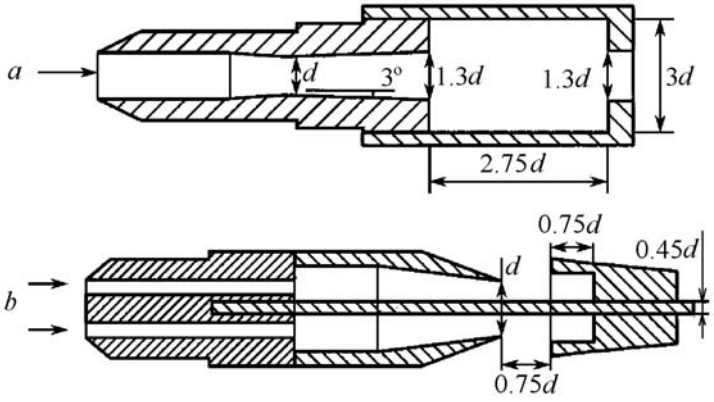

Fig. 3. Supersonic resonator nozzle (a) and the audio-frequency oscillator (b).

tube (Fig. 2) developed and manufactured under the supervision of R. I. Soloukhin. The experimental setup described in [4] consisted of a shock tube of square cross section, which was connected to a pressure chamber. The pressure chamber was fitted with optical glasses in two mutually perpendicular directions. Between the shock tube and the pressure chamber, there was a flange with the injectors under study. Flow visualization was carried out using an IAB-451 shadow device. Schlieren photographs showed the development of flow with an interval of 5 to 10 μs with an exposure time of 1 μs. Seventy-two 16×22 m^2 frames were produced in one experiment, using a VSK-5 high-speed camera. In flow-visualization experiments, the initial pressure and the Mach number behind the incident shock wave corresponded to the calculated values of these parameters and of the gas flow rate for detonation experiments. The pressure difference on the injectors varied 3.5 to 17 times.

A study was made of a supersonic nozzle, a resonator nozzle [5], and a Hartmann audio-frequency oscillator.

The resonator nozzle consisted of a supersonic nozzle rated at a Mach number of 2 and a coaxial resonator (Fig. 3a). The nozzle itself was also used as an independent injector in detonation experiments. Interacting with the resonator, the supersonic jet flowing out of the nozzle excited instability modes in the jet. These modes formed a strong acoustic field in the surrounding space and were dependent on the jet velocity and the resonator's dimensions.

The Hartmann oscillator represented a supersonic nozzle and a resonator (tube with a closed end, Fig. 3b). The possibility of generating acoustic waves and their intensity were determined by the distance between the nozzle and the resonator and were controllable.

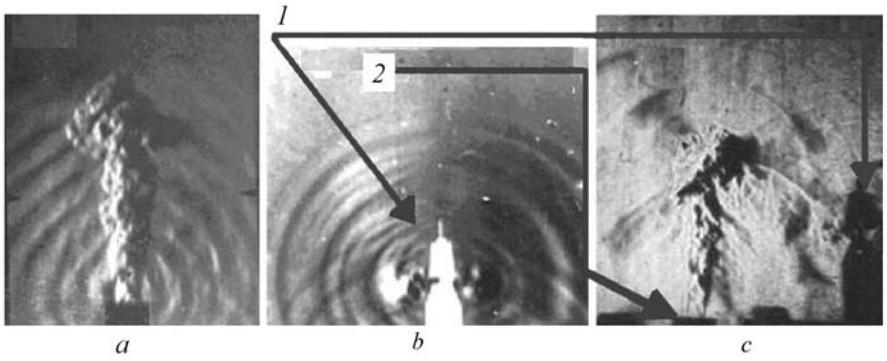

Fig. 4. Shadow photographs of gas outflow through a supersonic resonator nozzle (a), an audio-frequency oscillator (b), and a supersonic nozzle (c): 1) Hartmann oscillator; 2) supersonic nozzle.

Fig. 5. Line of the contact surface of the jet.

Shadow photographs of gas flow through the resonator nozzle and the Hartmann oscillator are presented in Fig. 4. The flow pattern for the Hartmann oscillator which is an acoustic-wave source is presented in Fig. 4b. The observed frequency of generation of acoustic waves acting on the flow of a supersonic jet was measured from schlieren photographs in outflow into air and was 27 kHz for the resonator nozzle and about 20 kHz for the Hartmann oscillator. The velocity of sound was measured from experiment from the known interframe time in high-speed photographing. Its value behind the primary shock wave was somewhat higher than the velocity in an unperturbed medium and corresponded to a gas temperature of about 380 K.

The schlieren photographs obtained with the high-speed photographing were processed with Adobe Photoshop to clearly identify the jet boundaries. Since the knife in the schlieren system was set up in parallel to the flow axis, the jet boundaries in the schlieren photographs were colored differently to the left and to the right of the flow axis. The side of best visibility of the boundary where it was prominent was selected. Then the contact-surface line was broken into segments of different curvature (Fig. 5). The area was calculated as the sum of all surfaces formed by the rotation of these segments about the flow axis.

The contact-surface area differed significantly for different types of injectors: the supersonic nozzles and the Hartmann oscillator.

Installation of the Hartmann oscillator near a supersonic nozzle can excite the boundary layer in a supersonic jet (Fig. 4c) and substantially increase the contact-surface area.

The periodic regime of outflow of the gas through the Hartmann oscillator was an additional problem. Figure 6 gives photographs of flow for certain time intervals. The photographs in Fig. 6a and b correspond to the first generation cycles, where the contact surface is seen quite clearly. In the cycles that follow, the injected and ambient gases are well mixed; therefore, it is impossible to identify the contact surface of the preceding cycles. It is only seen for

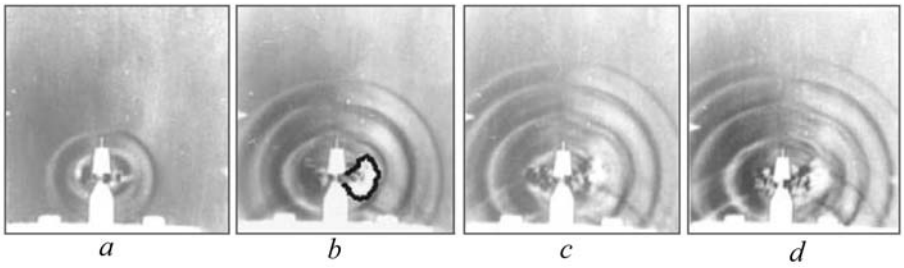

Fig. 6. Shadow photographs of flow out of the audio-frequency oscillator at an ambient pressure of 1 atm and a pressure difference of 6.15 on the injector at instants of time of 72 (a), 156 (b), 192 (c), and 228 μs (d) from the beginning of the outflow.

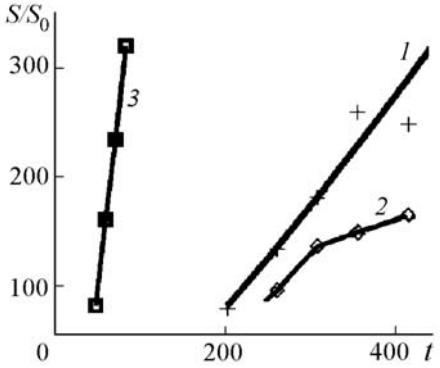

Fig. 7. Areas of the contact surface of the jet from the injectors vs. outflow time at a pressure difference of 6.6 on the injector and a flux of 33.1 g/s: 1) supersonic resonator nozzle; 2) supersonic nozzle; 3) audio-frequency oscillator. t, μs.

the running and previous generation cycles (Fig. 6b and c); therefore, its area was only computed for the first generation cycles (Fig. 7, curve 3).

For the nozzle with a resonator and without it, the areas of the contact surface of the formed jets with identical initial parameters strongly differ (Fig. 7, curves 1 and 2). However, for outflow from the Hartmann oscillator, the area of the jet surface (curve 3) is much larger than that in outflow from the resonator nozzle for the same initial parameters of the gas (curve 1).

After the preliminary visualization, the injectors were placed in the injector unit 2 (see Fig. 1) of a DCCh 1. The predetonation parameters and values of pressure in the front of a supercompressed detonation wave, the wave velocity on the portion of formation, and the velocities of the combustion front and the retonation wave (RW) were obtained for each type of injector.

Nozzles with resonators, nozzles without resonators, and Hartmann oscillators were also tested during the investigation of the influence of mixing on the formation of detonation. Cylindrical channels of throat area S_0 equal to the area of the remaining injectors were used as the simplest injectors.

Detonation was initiated by a spark discharger arranged at a distance of 150 mm from the injector unit. The stored electric energy in experiments with different types of injectors was 30 J. Before the experiment, the fuel and the oxidant were pumped into the buffer vessels 7 (Fig. 1) and were fed to the injectors through pressure-operated electric valves via tubes with a cross section larger than the total throat area of the injectors. Air at atmospheric pressure and a temperature of 293 K was initially present in the combustion chamber. After the opening of the valves, a mixture with a prescribed stoichiometric excess-fuel coefficient defined as the "equivalent relation" (ER) was formed in the DCCh and filled the DCCh to a certain pressure. The air initially present in the combustion chamber was displaced to the damping vessel. Initiation was carried out within 50 ± 4 ms after the opening of the valves. The valves were open at the instant of initiation. The RSV 113A34 pressure transducers and the FD 256 photodiodes were in-

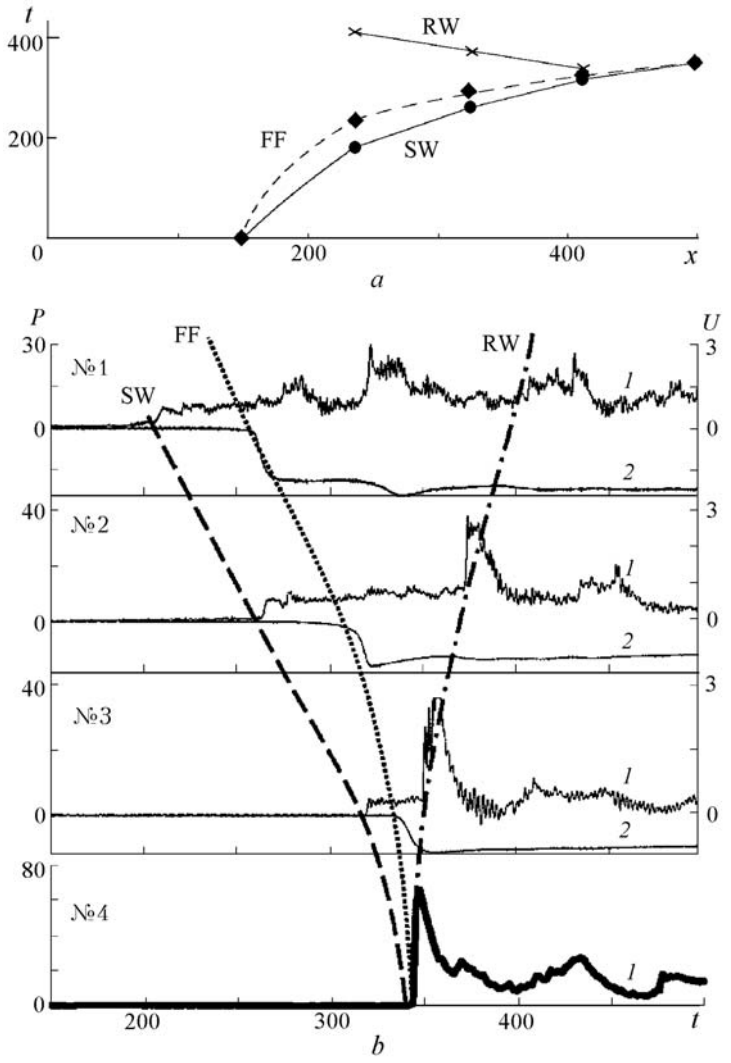

Fig. 8. *X–t* diagram (a) and the oscillograms of the pressure transducers (1) and photodiodes (2) in four successive cross section Nos. 1, 2, 3, and 4 at distances of 87, 174, 261, and 348 mm from the spark discharger (b) at ER = 2.4. *t*, μs; *x*, mm; *P*, atm.

stalled, along the DCCh, at equal distances from the discharger: 87, 174, 261, and 348 mm. Supersonic resonator nozzles were used as the injectors. Figures 8 and 9 give the oscillograms of the pressure transducers and the photodiodes. The time was reckoned from the instant of initiation. The stoichiometric relation between hydrogen and oxygen was calculated as the average one over the DCCh, disregarding the air present in the tube initially. The error in determining the flow rate of the mixture capable of detonation was no higher than 15%.

The formation of detonation was observed in the hydrogen–oxygen mixture with stoichiometric excess-fuel coefficient ER = 2.4 (Fig. 8) and 2.05 (Fig. 10b). The shock wave (SW) and the flame front (FF) were recorded by the pressure transducers (Fig. 8b, left-hand axis) and the photodiodes in relative units. When the resonator nozzles were used, the transducers in the third cross section recorded a lag of 9 μs of the flame front behind the shock wave (Fig. 8b). The retonation wave was recorded with a delay as a simultaneous increase in the pressure and the luminous flux (RW curve in Fig. 8a and b), which propagated in the direction of the closed DCCh end. Deflagration-to-detonation transition was observed between the third and fourth cross sections (Fig. 8). Detonation combustion was only observed in the fourth cross section.

Figure 9 shows the oscillograms of pressure and luminous flux in the second reference cross section at ER = 2.05 in feeding of the components through supersonic nozzles, supersonic resonator nozzles, and audio-frequency oscil-

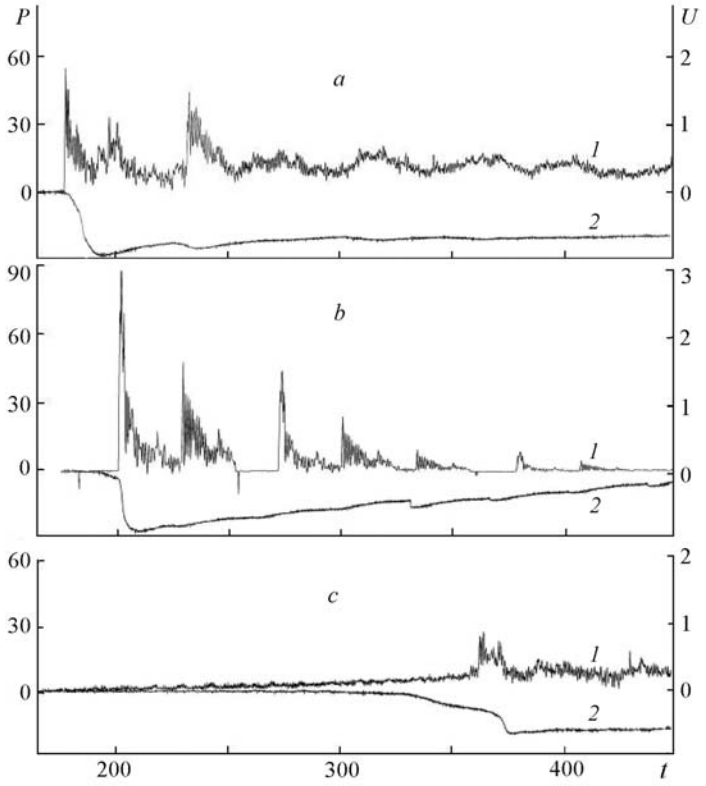

Fig. 9. Readings of the pressure transducers (1) and photodiodes (2) in the second reference cross section in feeding of the fuel components through supersonic nozzles (a), supersonic resonator nozzles (b), and the audio-frequency oscillator (c) at ER = 2.05. *P*, atm; *U*, V; *t*, μs.

lators respectively. When the resonator nozzles were used as the injectors, the peak pressure was markedly higher than that in feeding of the fuel components through the supersonic nozzles (Fig. 9a and b) but the wave velocity was lower. When the fuel components were fed through the audio-frequency oscillators the jet was directed perpendicularly to the chamber axis unlike the jets from the nozzles. In this case, the shock wave propagated much more slowly than with other injectors (Fig. 9c) despite the fact that the mixing surface was larger in this case. This effect was attributable to the frequency regime of flow of the gas out of the Hartmann oscillator. As a consequence, the composition of the fuel mixture was inconsistent with the calculated value.

The average velocities of propagation of the shock wave in the combustion chamber are shown as dashed lines in Fig. 10. This figure also shows the values of peak pressures along the chamber. When the fuel components were fed through the supersonic resonator nozzles, the peak pressure was markedly higher than the Chapman–Jouguet pressure (Fig. 10b). When the fuel components were fed through the audio-frequency oscillators the velocities of the shock wave and the flame front dropped behind the second reference cross section and did not attain the Chapman–Jouguet velocity (Fig. 10c).

In this series of experiments, a study was made of the influence of additional flow turbulization by changing the injector structure on the formation and parameters of detonation. The experiments have shown that for the stoichiometric excess-fuel coefficient ER = 0.5–2, the additional flow turbulization using the resonators on injectors influences the formation pattern and parameters of detonation only slightly. The formation of detonation is markedly accelerated only at ER = 2.3. Because of the insufficient sensitivity of the experimental procedure, no influence is found for nearly unity ERs.

The variability of the flow rate of the fuel components with time results in a changed proportion of the components in the process of DCCh filling with the fuel mixture (Fig. 11). A mixture less capable of detonation (with a larger ER) enters the spark-discharger region with time. The limiting value of the energy of initiation of the detonation

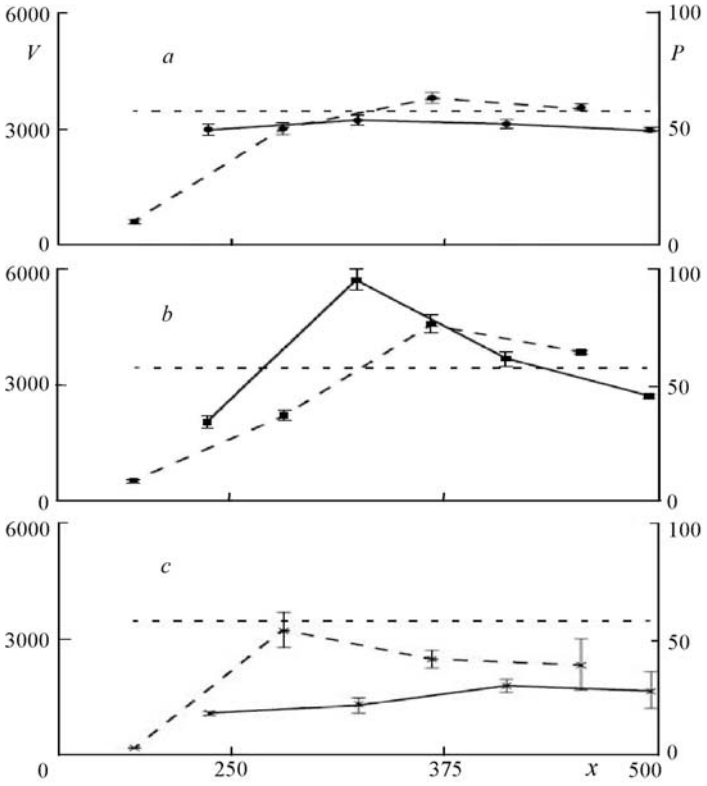

Fig. 10. Pressures in the detonation-wave fronts (solid curves) and the average velocities (dashed curves) in four successive cross sections in feeding of the reagents through supersonic nozzles (a), supersonic resonator nozzles (b), and the audio-frequency oscillator (c). The horizontal dashed line shows the parameters of Chapman–Jouguet detonation. V, m/s; P, atm; x, mm.

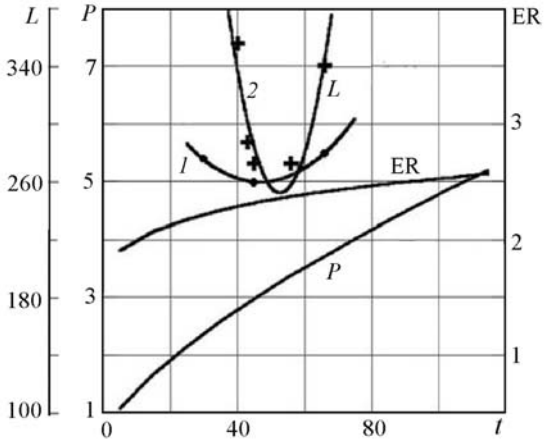

Fig. 11. Predetonation distance L, molar excess fuel ER, and initial pressure P in the combustion chamber vs. delay of initiation of the fuel mixture in feeding of the fuel components through supersonic nozzles: 1) with resonators; 2) without resonators. L, mm; P, atm; t, μs.

of the injected mixture entering the spark-discharger region increases with injection period. The predetonation length increases, too. At the same time, the growth in the fuel-mixture's initial pressure causes the predetonation length to diminish. Simultaneous action of two oppositely directed factors brings about the interval of optimum times of initiation delay.

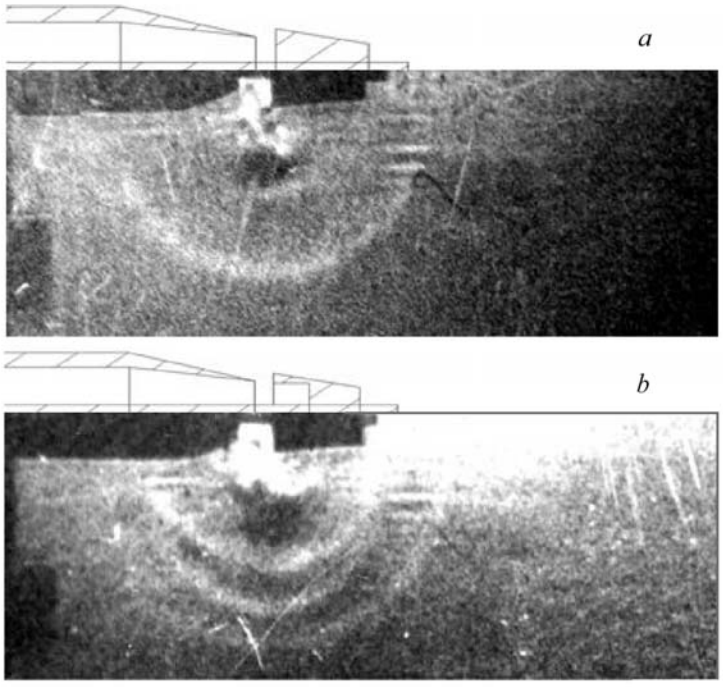

Fig. 12. Radial injectors with stationary outflow (a) and the Hartmann audio-frequency oscillator (b).

When the components are injected through the resonator nozzles at the design ER = 2.3, the optimum time interval of ignition delay lies within 40–43 ms; as ER increases to 2.6, the lower bound of the optimum interval is shifted to 65 ms. This result confirms the assumption that the parameters of the fuel mixture in the region of location of the spark discharger change in the process of filling of the DCCh.

When the components are fed through the supersonic nozzles at the design ER = 2.3, the optimum time interval of ignition delay is within 45–56 ms.

A study has been made of the influence of the mechanisms of feeding the reagents on deflagration-to-detonation transition with separate feed of the fuel and the oxidant. When the reagents were fed through the supersonic nozzles and resonator nozzles, detonation combustion in the hydrogen–oxygen mixture was attained at ER = 2.05 and 2.4 at a distance of less than 4 calibers of the combustion chamber. When the fuel components were fed through the audio-frequency oscillators, no detonation combustion was recorded in mixtures with ER = 2.05 and 2.4.

Influence of the Acoustic Action on the Ignition Region. The efficiency of external acoustic excitation of a supersonic jet was demonstrated in [6] using the elliptically focusing radiator. The nozzle was placed in the focus of an elliptic enclosure, whereas the gas oscillator producing sound was placed in the opposite focus. The maximum flow excitation was obtained for Strouhal numbers ranging from 0.25 to 0.30; a substantial increase in the contact-surface area was observed.

An additional set of radial injectors without a resonant cavity was developed and manufactured to investigate the influence of the acoustic field on the formation of detonation in the flow of miscible reagents. The parameters of outflow were selected so that the flow rate of the components, in feeding of the gases through the Hartmann audio-frequency oscillators and the radial injectors, was equal. The frequency of the appearing acoustic field was measured from the schlieren photographs taken with a VSK-5 high-speed camera. The visualization results have shown that the only difference in the flows from the injectors is in the presence of a strong acoustic field with a frequency of about 17 kHz in the case of flow of the gas out of the audio-frequency oscillator (Fig. 12). Consequently, we can speak of the analogous character of flows in the combustion chamber, and the differences in the development of combustion are attributable uniquely to the influence of the acoustic field [7].

Figure 13 plots the shock-wave velocity versus the distance along the tube axis at two pressures of the fuel mixture in the combustion chamber in the presence and in the absence of acoustic action.

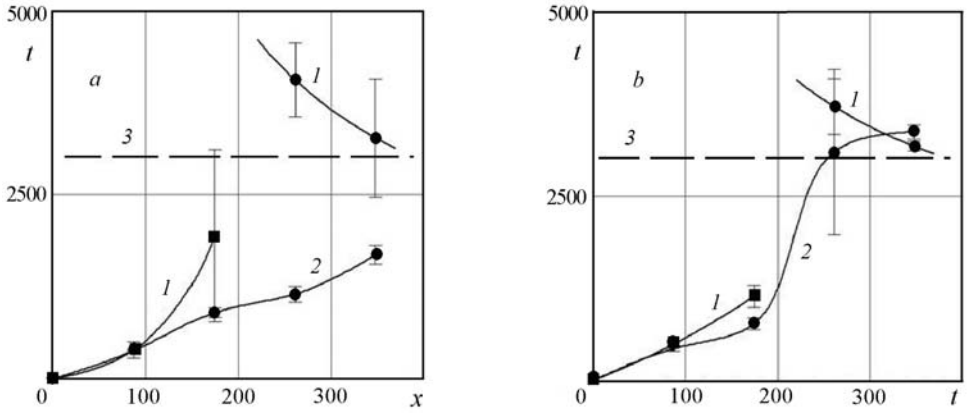

Fig. 13. Velocity distribution of the shock and detonation waves in the absence of the acoustic field (1) and in the presence of the acoustic field (2) at initial pressures of 1.4 atm (a) and 1.9 atm (b) in the combustion chamber (ER = 1.1); 3) Chapman–Jouguet detonation velocity. t, μs; x, mm.

The experiment has shown that in the absence of the acoustic action in the combustion chamber, detonation appears at a distance of about 2.5 combustion-chamber diameters from the ignition source (Fig. 13). In the presence of the acoustic field, the combustion-growth pattern is different: whereas at a pressure of 1.4 atm, the shock wave, by the end of the fourth caliber of the chamber, is accelerated to a velocity of about half the detonation wave, at a pressure of 1.9 atm the wave velocity at the same distance exceeds the stationary detonation velocity; nonetheless, it is noticeable that the acoustic action increases the length of formation of detonation. The negative influence of the acoustic field on the process of formation of detonation is more pronounced at a low pressure of the mixture capable of detonation in the tube than at a high pressure. This is due to the faster relaxation, at a low pressure, of large vortex structures and first ignition sites under the action of the acoustic field of the same intensity.

The acoustic field is known to be a packet of successively propagating weak compression and rarefaction waves. Such an action on a nonequilibrium turbulent flow contributes to the relaxation of large-scale vortex structures and to the transition of flow to an equilibrium turbulent one. Also, the acoustic field enhances the diffusion transfer of a substance, which leads to a relaxation of the gradients of pressure, temperature, and concentrations of active radicals. At the initial instant, this influences the development of combustion only slightly, since the temperature and concentration gradients of the active radicals are small, but at the instant preceding the formation of detonation, when first ignition sites are formed, the enhancement of relaxation processes leads to a decay of "hot spots," retarding the formation of detonation.

Reduction in the Predetoriation Length in the Flow of a Mixture Capable of Detonation. The experimental bench described above allowed experiments in both a moving and a quiescent mixture. The velocity of the unreacted mixture along the axis of the detonation chamber could attain 60 m/s, whereas the flow rate attained 0.6–0.8 liter/ms [8]. Reynolds numbers were as large as 10^5.

The presence of turbulence caused sharp acceleration of the flame front and led to a reduction in the predetonation period. Characteristic X–t diagrams of detonation formation in a quiescent and moving stoichiometric hydrogen–oxygen mixture at initiation energies of $\sim 0.1E_{cr}$ are given in Fig. 14, where the coordinate of the site of ignition is taken to be zero on the $0X$ axis. It is seen from the figure that in the moving mixture, the predetonation period and the predetonation length were reduced more than 8 times: the predetonation period was reduced from 2400 ± 200 μs to less than 220 μs, and the predetonation length was reduced from 700 ± 50 mm to less than 87 mm.

In the stoichiometric hydrogen–air mixture, detonation was initiated at initiation energies of $0.2–1.5E_{cr}$, where E_{cr} = 44.8 kJ/m^2 was the energy of direct initiation of detonation. Figure 15 gives the velocity distributions of shock/detonation waves along the DCCh axis for several initiation energies in the case of a quiescent mixture and in the case of a mixture moving with a velocity of 50 m/s.

In initiating detonation in the quiescent mixture, we observed two scenarios of detonation formation: monotonic increase in the shock-wave velocity, which was accompanied by the appearance of detonation at an initiation en-

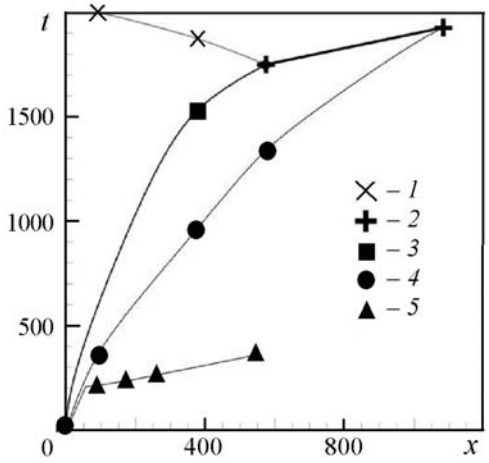

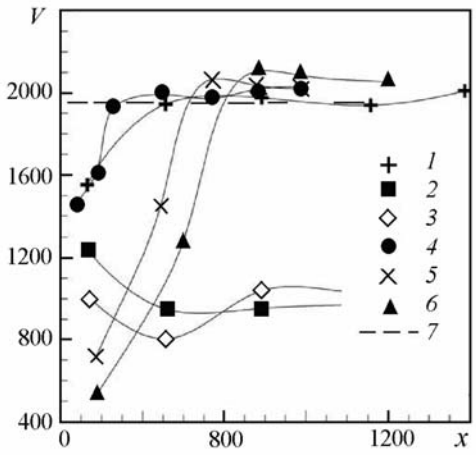

Fig. 14. Diagram of the deflagration-to-detonation transition in a quiescent (1–4) and moving (5) hydrogen–oxygen mixture: 1) retonation wave; 2) detonation wave; 3) flame front; 4) shock wave; 5) detonation wave in a moving mixture. t, μs; x, mm.

Fig. 15. Velocities of the shock and detonation waves in a quiescent stoichiometric mixture (1–3) and a mixture moving with a velocity of 50 m/s: 1) $E = 1.35E_{cr}$, 2) $0.97E_{cr}$, 3) $0.65E_{cr}$, 4) $0.81E_{cr}$, 5) $0.5E_{cr}$, and 6) $0.25E_{cr}$, 7) Chapman–Jouguet detonation velocity. V, m/s; x, mm.

ergy higher than $0.5E_{cr}$, and decrease in the shock-wave velocity followed by its increase. However, in initiating detonation in the moving mixture at initiation energies more than $0.2E_{cr}$, the velocity of the primary shock wave grew in propagation along the axis of the combustion chamber. The predetonation length was reduced more than fourfold: to 600 mm at $E = 0.5E_{cr}$ and to 800 mm at $E = 0.25E_{cr}$.

The influence of the position of the site of ignition of a mixture capable of detonation on the formation of detonation was investigated in the stoichiometric hydrogen–oxygen mixture at initial pressures of 1 and 3 atm. The initiation energy was varied from $0.001E_{cr}$ to $0.2E_{cr}$. We measured predetonation lengths, which are plotted in Fig. 16 versus the position of the spark discharger relative to the injector unit.

It follows from the results obtained that the predetonation length L_{ddt} attains its maximum at $L/d = 1.2$. At $L \approx 1.2d$, the expanding combustion products initiate compression waves, which, being reflected from the closed DCCh end, catch up with the compression waves traveling in the direction from the end, additionally accelerating the unreacted gas. This leads to its additional turbulization, to an acceleration of the flame front, and finally to a reduction in the predetonation length. In the case where the discharger is located in close proximity to the closed DCCh end ($L \approx 0.2$–$0.3d$) compression waves are initiated only in one direction. There are no reflected waves and hence no additional turbulization. At $L \approx 2d$, the reflected compression waves do not manage to catch up with the compression waves moving in the direction from the end before the onset of detonation.

Also, it has been found that at initiation-energy densities lower than $0.02E_{cr}$, the onset of detonation is substantially influenced by the position of the site of ignition relative to the closed DCCh end. The lower the energy density, the more pronounced the influence. At energy densities higher than $0.08E_{cr}$, the influence of the initiator on the medium becomes so strong that the position of the initiation site is immaterial. At intermediate values of energy, the displacement of the discharger position influences only the predetonation period.

However, the conclusions mentioned above are only true for quiescent mixtures, since when a moving stoichiometric hydrogen–oxygen mixture is ignited the propagation of the flame is significantly influenced by flow turbulization. The detonation wave can be initiated much closer to the initiation source at distances of 0.5–2 calibers from it.

Influence of the Magnetic Field on the Characteristics of Spark Discharge in Initiation of Detonation. One method of diminishing the predetonation length and reducing the initiation time of detonation isto increase the ig-

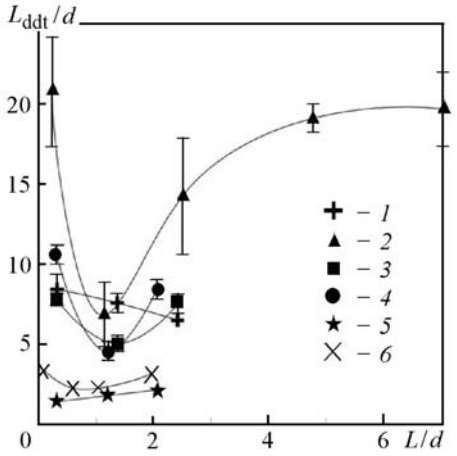

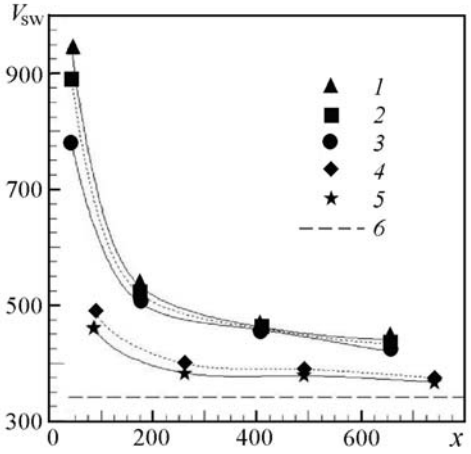

Fig. 16. Predetonation length L_{ddt}/d vs. position of the spark discharger L/d: 1) d = 83 mm, P = 1 atm, E_{cr} = 20 J, and $E_{disch} = 0.2E_{cr}$; 2) d = 22 mm, P = 1 atm, E_{cr} = 1.4 J, and $E_{disch} = 0.2E_{cr}$; 3) d = 83 mm, P = 1 atm, E_{cr} = 20 J, $E_{disch} = 0.1E_{cr}$; 4) d = 83 mm, P = 1 atm, E_{cr} = 20 J, and $E_{disch} = 0.006E_{cr}$; 5) d = 83 mm, P = 3 atm, E_{cr} = 6.7 J, and $E_{disch} = 0.009E_{cr}$; 6) d = 22 mm, P = 3 atm, E_{cr} = 0.5 J, and $E_{disch} = 0.03E_{cr}$.

Fig. 17. Velocity distribution of the shock wave along the DCCh axis: 1) E = 900 and B = 1.5, 2) 900 and 0, 3) 900 and −1.5, 4) 200 and 1.5, and 5) 200 J and 0 T; b) velocity of sound. V_{sw}, m/s; x, mm.

nition power. In the case where initiation is effected by a spark discharge, the influence exerted on it by the magnetic field can be substantial.

Investigation of the influence of the magnetic field on the plasma region of electric discharge was carried out in three steps [9]. In the first step, we visualized a spark discharge in air at atmospheric pressure with simultaneous operation of two dischargers. One discharger was exposed to a magnetic field produced by the discharge current itself in the conductor in close proximity to the discharge gap. It has been shown in the work that the plasma region near the discharger increases in the presence of the magnetic field and the shock-wave velocity grows 10% in the initial step.

In the second step, the influence of the magnetic field on the electric discharge was investigated in the DCCh described above. The magnetic field was produced using two induction coils arranged beyond the DCCh on both sides of the spark discharger, whereas the stored energy was 6 or 3 kJ. The stored electric energy delivered to the spark discharger was varied from 0.20 to 1.56 kJ. The electrodes of the spark discharger within the DCCh were arranged so that the direction of the discharge current was perpendicular to the magnetic field. This maximized the influence of the magnetic field on the current. The velocity distributions of the shock waves along the axis of the combustion chamber, created by the spark discharger, are given in Fig. 17 for several energies of this discharge. When the directions of the external magnetic field and the self-magnetic field of the spark discharger were coincident, the shock-wave velocity increased by 50 m/s; for the opposing directions of the external magnetic field and the self-magnetic field of the spark discharger, the shock-wave velocity diminished by 100 m/s.

Calculation from the Biot–Savart–Laplace formula has shown that under these conditions, when the directions of the vectors of the external magnetic (induction coils beyond the DCCh) and self-magnetic (magnetic induction of the spark current) fields are coincident, the magnetic induction within the discharger increases from 2 to 2.7 T; in the case of their opposing directions it diminishes from 2 to 1.3 T.

In the third step, the influence of the magnetic field on the length of the predetonation portion in the hydrogen–air mixture (1 atm) was investigated for an electric energy of 0.9 kJ delivered to the spark discharger. When the external magnetic field (measured magnetic induction 1.5 T) whose direction was coincident with the direction of the self-magnetic field of the spark discharger was switched on, we observed the formation of supercompressed detonation at a distance of eight calibers. The transducers installed at a distance of 9 calibers from the discharger (Fig. 18) did not sense the lag of the flame front behind the shock wave, whereas without a magnetic field the primary shock wave

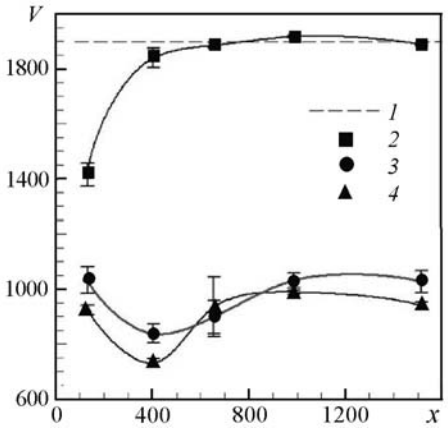

Fig. 18. Influence of the external magnetic field on the velocity of the shock wave induced by the electric discharge in the hydrogen–air mixture and on the process of deflagration-to-detonation transition: 1) Chapman–Jouguet detonation velocity; 2) B = 1.5, 3) 0, and 4) 1.5 T. V, m/s; x, mm.

was first attenuated but thereafter, after 7 calibers from the ignition site, began to build up again. However, in the DCCh of length 30 calibers, the flame front lagged behind the shock wave by 100 μs and no detonation was formed. The reversal of the direction of the magnetic-induction vector led to a reduction of 100 m/s in the velocity of the primary shock wave.

Thus, it has been shown that the imposition of the magnetic field on the discharge region influences the intensity of the shock wave; at a magnetic induction of 1.5 T, the predetonation length is reduced no less than five times. The established effect will make it possible to improve the efficiency and to diminish the dimension of promising devices in which detonation burning of fuel is used.

Improvement in the Efficiency of Electric-Discharge Initiation of Detonation by the Self-Magnetic Field. The influence of the self-magnetic field of the electric discharger on the parameters of denotation of a moving fuel–air mixture was investigated in a cylindrical combustion chamber of diameter 28 mm [10].

A flow of a fuel–air mixture with spraying of hexane was blown through the chamber. The temperature of the tube and the discharge chamber was maintained in the range 60–70^{o}C to ensure stable quality of the mixture. The recording pressure transducers were arranged at distances of 180, 580, and 980 mm from the discharger. The chamber made it possible to test different discharger structures. Several discharger structures were proposed and tested. With the aim of minimizing the loss, we selected a three-electrode circuit making it possible to trigger a discharge without an external switch. The initiating electrode ignited the auxiliary discharge with a current of the order 100 A, from which the basic discharge was triggered. The capacity of the storage battery and the voltage on it were selected so as to maximize discharge-energy transfer to the gaseous medium, i.e., to create the maximum intense shock wave. In discharger No. 1, the arc filament formed a straight line with power electrodes (Fig. 19). The arc filament did not interact with the magnetic field from the fed electrodes. To such a discharger, there was assigned 0 support turns.

Discharger No. 2 with a nearly closed additional turn formed by the power electrode set up an amplified magnetic field in the discharge region; therefore, 1 support turn was assigned to it (Fig. 20). At a maximum discharge current of 20 kA, the magnetic field with an induction of about 0.7 T was set up.

Discharger No. 3 was analogous to discharger No. 2 in design and contained two additional turns formed by power electrodes which were packed into the channel and sealed with epoxy resin. Three series-connected turns were formed together with the arc; they increased the magnetic field in the discharge region and "inflated the arc" due to the forces proportional to the current squared. The induction of the self-magnetic field of discharger No. 3 was about 1.5 T at a maximum current of 20 kA. Increasing the number of additional turns (and hence the induction of the self-magnetic field of the discharger) turned out to be inexpedient. The additional turns increased the induction of the discharge circuit and accordingly the discharge time, which caused the fraction of energy transferred to the gas by the discharge to substantially diminish. Figures 21–23 plot the wave velocities versus the electric energy stored in the capacitive storages for different structures of the discharger.

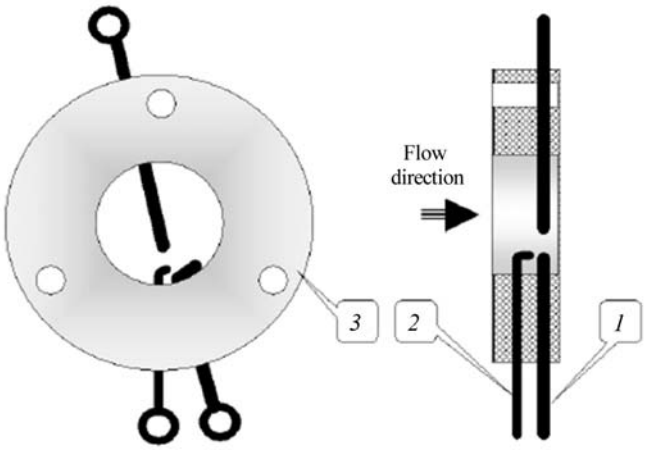

Fig. 19. Diagram of discharger No. 1 with a discharge gap of 7 mm: 1) power electrode; 2) initiating electrode; 3) casing manufactured from polycarbonate.

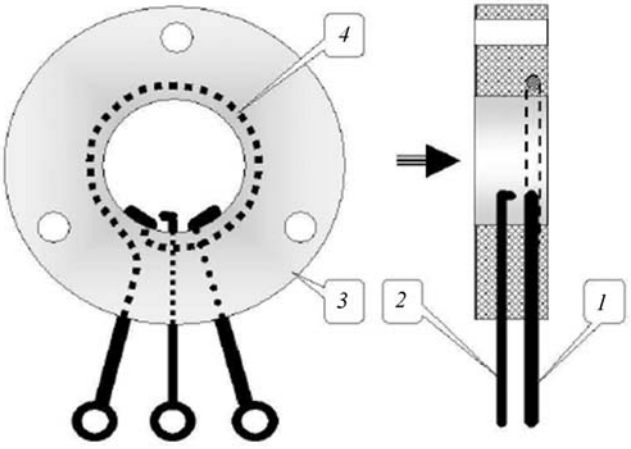

Fig. 20. Diagram of discharger No. 2 with a discharge gap of 7 mm. Notation 1–3 is the same as that in Fig. 19; 4) additional turn.

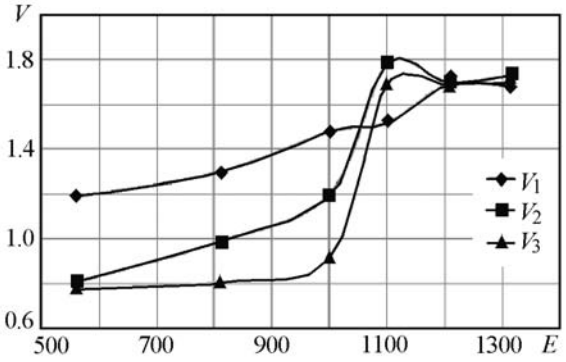

Fig. 21. Velocity of the wave produced by discharger No. 1 vs. stored energy: V_1, V_2, and V_3, velocities recorded by pressure transducers at distances of 180, 580, and 980 mm from the discharger. V, km/s; E, J.

Near the discharger, on the first base, the wave velocity V_1 is dependent on the storage energy quite smoothly, since it is mainly determined by the discharge energy. Away from the discharger, on the second and third bases, the dependence of the wave velocities V_2 and V_3 on the storage energy has an abrupt jump, since the velocity is determined by one of the two steady-state regimes — that of a damping wave or detonation. The detonation-initiation energy can be determined from the plots given in the figure as the energy at which the wave velocity away from the

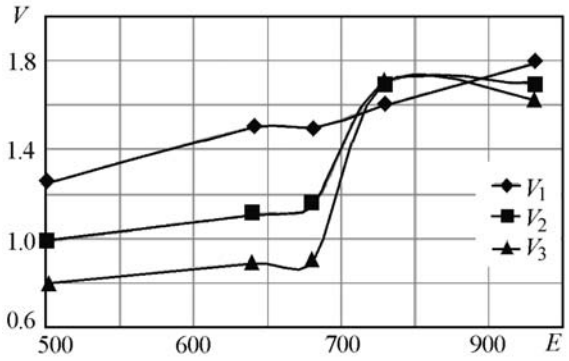

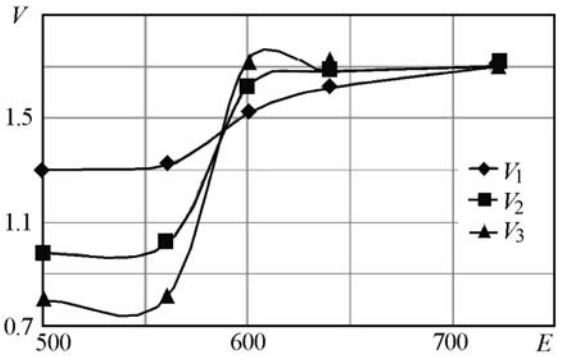

Fig. 22. Velocity of the wave produced by discharger No. 2 vs. stored energy. The notation V_1, V_2, and V_3 is the same as that in Fig. 21. V, km/s; E, J.

Fig. 23. Velocity of the wave produced by discharger No. 3 vs. stored energy. The notation V_1, V_2, and V_3 is the same as that in Fig. 21. V, km/s; E, J.

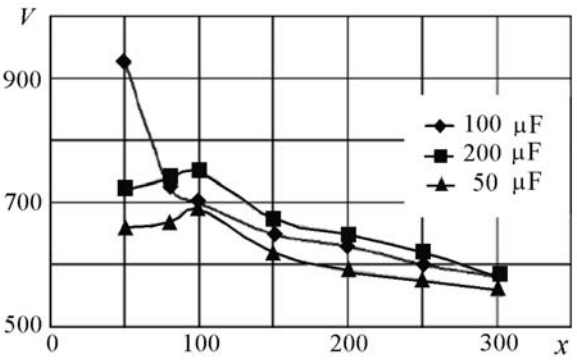

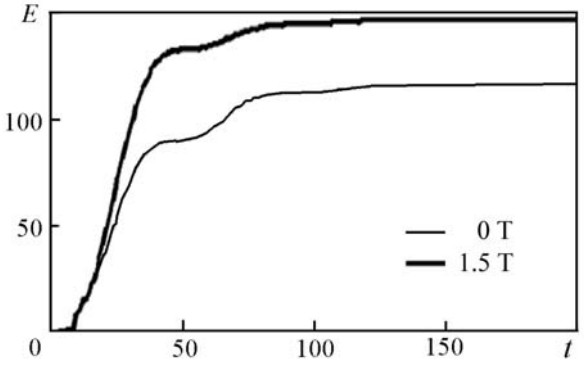

Fig. 24. Velocity distribution of the shock wave along the axis of the combustion chamber at a stored energy of 200 J and at several capacities of the capacitor. V, km/s; x, mm.

Fig. 25. Influence of the magnetic field on the value of the discharge-current work. E, J; t, μs.

discharger grows from 0.8–1.2 km/s to 1.7–1.8 m/s. The results of measurements of the energy necessary for initiating the detonation of a fuel–hydrogen mixture (as a function of the induction of the discharger's self-magnetic field) are given below:

B, T	E, J
0	1000–1100
0.7	690–710
1.5	560–580

We have measured the velocities of propagation of the shock wave in a dielectric tube of diameter 44 mm and length 400 mm filled with air at atmospheric pressure. The stored energy was 200 J. A knife pressure transducer was used for measuring the average wave velocity from the discharger to the mark x. It turned out that the maximum velocity of the shock wave (800 m/s) was attained with discharger No. 3, whereas the minimum velocity (670 m/s) was attained with discharger No. 1, where the influence of the self-magnetic field was virtually absent.

The influence of the capacity of storage batteries (with the same stored energy) on the intensity of the shock wave produced by the electric discharge was investigated. The tests performed have shown that the discharge efficiency drops at elevated supply voltages (and diminished capacities). The same conclusion has also been drawn for large capacities (and low voltages); the wave velocity measured in the dielectric tube is given in Fig. 24 as a function of the distance to the spark discharger.

TABLE 1. Calculation of the Discharge-Current Work

B, T	E_1, J	E_2, J	E_3, J	E, J	η, %
0	88	21	4	113	12.6
1.5	125	12	2	139	15.4

We obtained and processed the oscillograms of electric discharge for the discharger with an amplified self-magnetic field (of about 1.5 T) and without it; the stored electric energy was 900 J. The discharge voltage was measured using a voltage divider, whereas the discharge current was measured with a Rogowski loop with an integrator. The work E done by the current was computed as the time integral of the product of the discharge current and the spark-discharge voltage. The discharger efficiency η was determined as the ratio of the work of the discharge current $E(\tau)$ to the stored electric energy E_0, where τ is the discharge time. Figure 25 gives a calculation result: the work E as a function of the time.

Table 1 gives the calculations of the work E_1, E_2, and E_3 which correspond to three half-periods of variation in the discharge current with time. The efficiency of the discharger and the fraction of the energy transferred to the gas grow 20–25% in the discharger's self-magnetic field with an induction of 1.5 T.

Rough calculation has shown that the force (acting on the arc from the magnetic field) of the work done by the field in the process of "inflation" of the electric arc is linearly dependent on the number of additional turns and square-law-dependent on the current strength. At a stored energy of 700 J and a current of 20 kA, this work turns out to be equal to approximately 25 J. As has been noted above, only a small part of the stored energy (10%) passes into the gaseous mixture, whereas, according to the calculations, the effective discharge energy considerably grows when the amplified self-magnetic field of the discharger is used.

A nearly twofold reduction in the detonation-initiation energy with increase in the self-magnetic field of the spark discharger to 1.5 T has been experimentally found in the work.

Conclusions. The use of injectors with turbulizing and resonator elements leads to a change in the initial conditions for the development of the flame and the formation of detonation. Additional flow turbulization causes the predetonation length to reduce. The acoustic action on the ignition and combustion region retards the acceleration of the flame and the onset of detonation.

It has been found that in the flow of a mixture capable of detonation, detonation can be formed at a distance of several calibers of the combustion chamber at an initiation energy orders of magnitude lower than the critical energy of direct initiation of detonation; in a quiescent mixture, detonation formation is observed at a distance of more than 30 DCCh calibers at an initiation energy lower than the critical one.

The dependences of the predetonation length in the quiescent mixture and in the flow on the distance between the initiation source and the closed DCCh end have been obtained. The optimum location of the spark discharger in the DCCh for which the predetonation length is minimum has been determined.

The influence of the self-magnetic field of the spark discharger and the external induced magnetic field on the parameters of the electric discharge and detonation initiation in quiescent mixtures and in the flow at a mixture capable of detonation has been investigated. The imposition of the magnetic field on the discharge region increases the fraction of energy stored in the storage and released in the discharge gap, which leads to a substantial reduction in the predetonation length.

The authors express their sincere thanks to Professor T. V. Bazhenova for useful discussions. This work was carried out with partial support from the Russian Foundation for Basic Research (08-03-01089-a and 10-08-00214-a) and the RAS OÉ-1 program.

NOTATION

B, magnetic induction; d, inside diameter of the DCCh; E, ignition energy; E_1, E_2, and E_3, fractions of the discharge energy which correspond to three successive half-periods of the current; E_{cr}, critical energy of direct detonation initiation; ER, excess-fuel coefficient; L, distance from the closed end of the chamber to the ignition source; L_{ddt}, length of the deflagration-to-detonation transition; P, pressure in the shock/detonation-wave front; S, area of the

contact surface of the jet; S_0, injector throat area; t, time from the beginning of the process; U, output voltage of the light sensor; V, average velocity of propagation of the shock wave; V_1, V_2, and V_3, shock-wave velocities on three successive bases; V_{sw}, shock-wave velocity created by the spark discharger; x, position of the object on the axis of the combustion chamber; η, efficiency.

REFERENCES

1. R. I. Soloukhin, Detonation waves in gases, *Usp. Fiz. Nauk*, **80**, Issue 4 (1963).
2. V. V. Golub, Pulse detonation device: advantages, difficulties, and scientific problems, in: *Proc. 23rd Int. Symp. on Shock Waves*, 21–25 July 2001, Arlington, Texas, USA.
3. V. V. Golub and T. V. Bazhenova, *Pulse Supersonic Jet Flows* [in Russian], Nauka, Moscow (2008).
4. D. I. Baklanov, T. V. Bazhenova, T. A. Bormotova, V. V. Golub, A. A. Makeich, V. V. Volodin, D. M. Meiers, and F. K. Lyu, Investigation of the influence of mixing on deflagration-to-detonation transition, *Khim. Fiz.*, **22**, No. 8, 38–44 (2003).
5. E. J. Gutmark, K. C. Schadow, and K. H. Yu, *Ann. Rev. Fluid Mech.*, 195 (1995).
6. Y. Y. Borisov and N. M. Gynkina, *Sov. Phys. Acoust.*, **21**, No. 3, 230–233 (1975).
7. D. V. Blagodatskikh, V. V. Volodin, S. V. Golovastov, V. V. Golub, and M. F. Ivanov, Influence of acoustic waves on the zone of ignition and deflagration-to-detonation transition: Experiment and calculation, *Teplofiz. Vys. Temp.*, **47**, No. 2, 315–316 (2009).
8. D. I. Baklanov, V. V. Volodin, S. V. Golovastov, and V. V. Golub, Appearance of detonation in a flow of a combustible mixture, *Khim. Fiz.*, **24**, No. 7, 5–7 (2005).
9. V. V. Golub, V. S. Aksenov, D. I. Baklanov, V. V. Volodin, S. V. Golovastov, S. A. Gubin, V. P. Efremov, A. S. Savel'ev, V. E. Fortov, and Yu. L. Sharov, Investigation of the influence of a magnetic field on the initiation of detonation by a spark discharge in a hydrogen-air mixture, *Dokl. Ross. Akad. Nauk*, **404**, No. 3, 326–328 (2005).
10. A. S. Savel'ev, V. S. Aksenov, S. A. Gubin, V. V. Golub, and V. P. Efremov, Efficiency of initiation of gaseous detonation by an electric discharge and a magnetic field, in: *The Physics of Extremal States of a Substance* [in Russian], Chernogolovka (2007), pp. 154–156.